Current Research in Structural Biology 3 (2021) 41–50

Contents lists available at ScienceDirect

Current Research in Structural Biology

journal homepage: www.journals.elsevier.com/current-research-in-structural-biology

Integrated analysis of Shank1 PDZ interactions with C-terminal and internal binding motifs

Muhammad Ali [a], Mishal Mariam McAuley [b,c], Susanne Lüchow [a], Stefan Knapp [b,c], Andreas C. Joerger [b,c,**], Ylva Ivarsson [a,*]

[a] Department of Chemistry – BMC, Uppsala University, Husargatan 3, 751 23, Uppsala, Sweden
[b] Institute of Pharmaceutical Chemistry, Goethe University Frankfurt, Max-von-Laue-Str. 9, 60438, Frankfurt am Main, Germany
[c] Structural Genomics Consortium (SGC), Buchmann Institute for Molecular Life Sciences (BMLS), Max-von-Laue-Str. 15, 60438, Frankfurt am Main, Germany

ARTICLE INFO

Keywords:
PDZ domain
Phage display
Short linear motif
SLiM
PDZbm
Shank
ARAP3

ABSTRACT

PDZ domains constitute a large family of modular domains that are well-known for binding C-terminal motifs of target proteins. Some of them also bind to internal PDZ binding motifs (PDZbms), but this aspect of the PDZ interactome is poorly studied. Here we explored internal PDZbm-mediated interactions using the PDZ domain of Shank1 as a model. We identified a series of human Shank1 ligands with C-terminal or internal PDZbms using proteomic peptide-phage display, and established that while the consensus sequence of C-terminal ligands is x-T-x-(L/F)–COOH, the consensus of internal PDZbm is exclusively x-T-x-F-x, where x is any amino acid. We found that the affinities of PDZbm interactions are in the low micromolar range. The crystal structure of the complex between Shank1 PDZ and an internal PDZbm revealed that the binding mode of internal PDZbms was similar to that of C-terminal ligands. Pull-down experiments confirmed that both C-terminal and internal PDZbm interactions can occur in the context of full-length proteins. Our study expands the interactome of Shank1 and hints at a largely unexplored interaction space of PDZ domains.

1. Introduction

The PDZ (PSD-95/DLG/ZO-1) domain is one of the most common modular domains in the human proteome with more than 260 occurrences in over 150 proteins (Ivarsson, 2012; Luck et al., 2011). Despite being a highly studied module, the plasticity of its interactions remains enigmatic. PDZ domains typically bind to C-terminal PDZ binding motifs (PDZbms) (Ernst et al., 2014; Songyang et al., 1997; Stiffler et al., 2007; Tonikian et al., 2008), but some of them also bind so-called internal PDZbms. The internal PDZbms may be located in the intrinsically disordered regions of target proteins, like most short linear binding motifs of the proteome (Tompa et al., 2014), but they may also be found in structured regions, such as in the case of the nNOS-syntrophin complex, where formation of a beta-hairpin enables the internal PDZbm in nNOS to bypass the normal requirement for a COOH-terminus and dock into the syntrophin PDZ peptide binding groove (Hillier et al., 1999; Penkert et al., 2004; Zhang et al., 2009). Adding to the complexity, PDZ-ligand interactions may be regulated or tuned by phosphorylation of PDZ domains or the PDZbms (Gogl et al., 2019; Sundell et al., 2018). PDZ domains of peripheral membrane proteins may also bind to the headgroups of membrane phospholipids (Gallardo et al., 2010; Ivarsson et al., 2013), which may compete with peptide binding or may fine-tune the affinity for the peptide ligand (Ivarsson et al., 2013; Egea-Jimenez et al., 2016). Despite being rather simple binding modules, PDZ domains thus exhibit a high plasticity of interactions.

Here, we have explored the internal PDZ-bm interactions using Shank (SH3 and multiple ankyrin repeat domains protein) 1 as a model system. Shank proteins are major scaffolding proteins located at the postsynaptic density that are crucial for synaptic function. The three Shank protein homologues (Shank1, 2 and 3) are composed of N-terminal ankyrin repeats followed by an SH3 (Src homology 3) domain and a PDZ domain that engages in interactions with several other proteins (Fig. 1A). Mutations in Shank proteins and their ligands are associated with psychiatric disorders, such as autism spectrum disorder and schizophrenia (Leblond et al., 2014; Peca et al., 2011; Soler et al., 2018). To understand the role of disease-related mutations of Shank proteins, it is necessary to explore

* Corresponding author.
** Corresponding author. Institute of Pharmaceutical Chemistry, Goethe University Frankfurt, Max-von-Laue-Str. 9, 60438, Frankfurt am Main, Germany.
E-mail addresses: Joerger@pharmchem.uni-frankfurt.de (A.C. Joerger), ylva.ivarsson@kemi.uu.se (Y. Ivarsson).

https://doi.org/10.1016/j.crstbi.2021.01.001
Received 12 November 2020; Accepted 2 January 2021

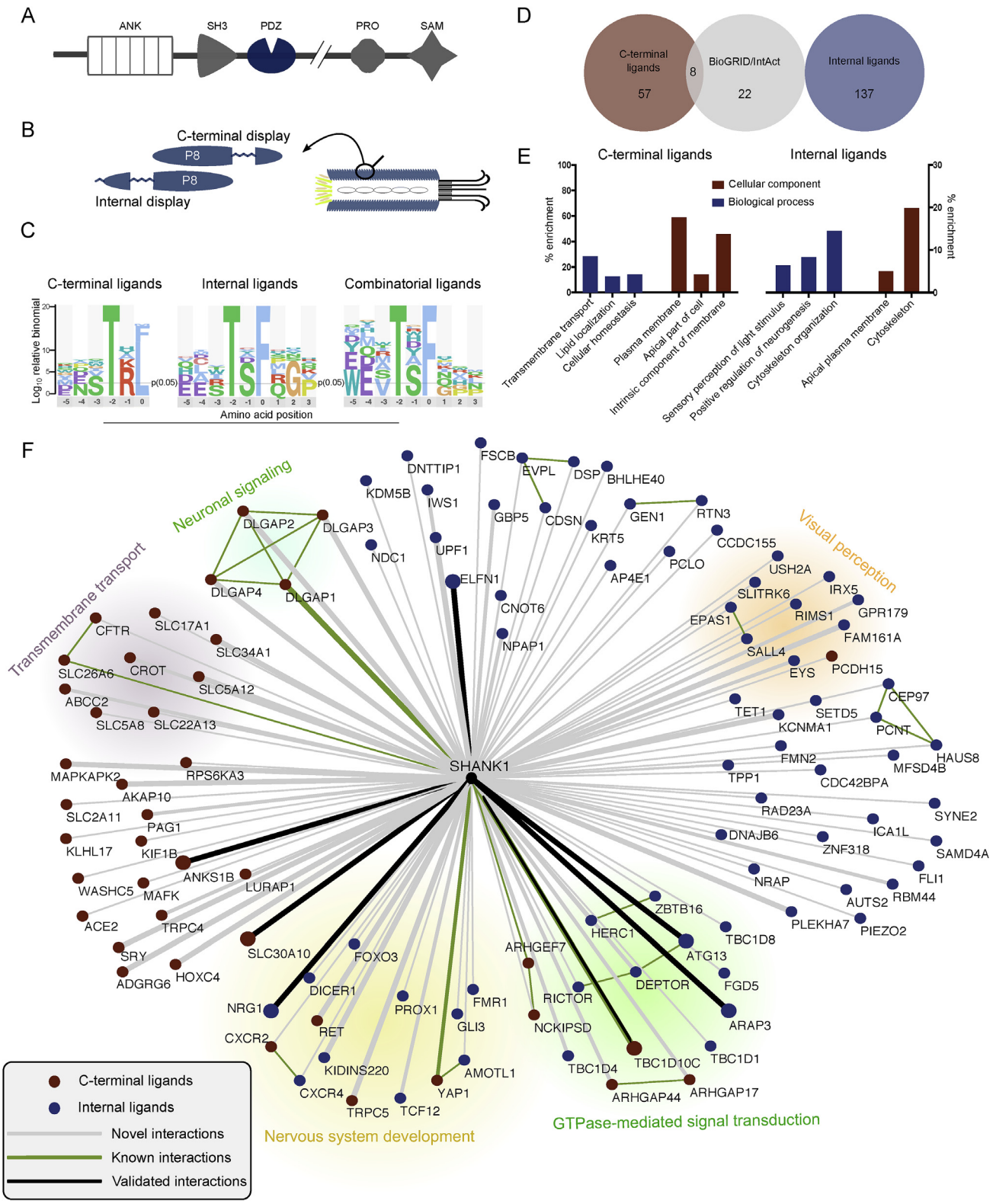

Fig. 1. Phage display against Shank1 PDZ identifies consensus motifs and expands the potential interactome. (A) Schematics of the domain organization of Shank1. (B) The peptide-phage libraries used in the study displayed peptides C-terminally or N-terminally of the major coat protein P8 of the M13 phage. (C) Schematic of position-specific scoring matrices (PSSMs) representing the binding-enriched sequences from C-terminal ProP-PD, N-terminal (internal) ProP-PD, and combinatorial peptide-phage display. (D) Comparison between ProP-PD hits and Shank1 interactions reported in BioGRID and IntAct (April 2020). (E) Enriched GO terms of high-confidence ProP-PD ligands based on DAVID GO term analysis. (F) Network view of identified Shank1 PDZ ligands that share GO terms with Shank1 that are unlikely to occur by chance ($p < 0.01$). Ligands from the C-terminal and internal selections are indicated by red and blue circles, respectively. Previously reported interactions are indicted with green lines. Interactions validated in this study are indicated with black connecting lines. The width of the lines represents the relative NGS counts for the peptide hits from ProP-PD selections. The background colors highlight relevant biological roles in the cell. The network was created using Cytoscape 3.7.

the molecular determinants of their bimolecular interactions. The PDZ domains of Shank1-3 bind to a variety of ligands with C-terminal class I PDZbms (x-S/T-x-(L/F)–COOH, where x indicates any amino acid). Known C-terminal Shank1 ligands include the DETNL-COOH peptide from β-PIX (ARHGEF7) (Lee et al., 2011), which is a guanine nucleotide exchange factor for the GTPases Rac1 and Cdc42, and the AQTRL-COOH peptide from disks large-associated proteins (DLGAPs) (Im et al., 2003), which is a part of the postsynaptic scaffold in neuronal cells. A binding site outside of the canonical PDZ domain also contributes to the affinity and specificity of DLGAP for the homologous Shank3 protein, which strongly favors formation of this high-affinity complex over interaction with other potential Shank targets in synapses (Zeng et al., 2016). Additionally, Shank1 PDZ recognizes internal PDZbms, as first shown for the glutamate receptor ionotropic, delta-2 (Grid2) (Uemura et al., 2004). More recently, phage display screening suggested that Shank1 PDZ may bind to a large number of internal PDZbms in the human proteome, but none of the suggested interactions has been validated so far (Davey et al., 2017).

In this study, we explored the interactions of the Shank1 PDZ domain with C-terminal and internal PDZbms through proteomic peptide-phage display (ProP-PD) using two distinct phage peptidomes; one that represents the C-terminal regions of the proteome and the other that displays intrinsically disordered regions of the human proteome (Davey et al., 2017; Ivarsson et al., 2014). In line with previous results, we found that the C-terminal and internal PDZbms are similar, but yet distinct. In particular, the requirements for internal PDZbms for binding Shank1 PDZ are more stringent. Affinity determinations revealed that the Shank1 PDZ domain binds C-terminal and internal PDZbms with low-to-mid micromolar affinities, while the C-terminal peptides showed generally stronger interactions. The structure of Shank1 PDZ in complex with the internal PDZbm of ARAP3 revealed that the overall binding modes of the C-terminal and internal PDZbms are more or less identical, but with small differences in the carboxylate-binding loop interactions that account for differences in binding affinities. We further confirmed that both C-terminal and internal PDZbms can interact with Shank1 PDZ in the context of their full-lengths proteins. The results suggest that the interactome of Shank1 is preferentially based on interactions with C-terminal ligands but also includes interactions with ligands having internal PDZbms, which also may apply to other members of the large PDZ domain family.

2. Results and discussion

2.1. Identification and analysis of Shank1 PDZ ligands through ProP-PD and bioinformatic analysis

We explored the C-terminal and internal PDZbm-based interactome of Shank1 PDZ through ProP-PD selections. ProP-PD is a variant of phage display where the displayed peptide libraries are designed based on a proteome of interest. Here, we used i) a heptameric C-terminal phage peptidome containing more than 50,000 C-terminal peptides from the human proteome (Ivarsson et al., 2014), and ii) an internal phage peptidome designed to display close to 500,000 16-amino acid long peptides representing the intrinsically disordered regions of the human proteome flanked by flexible G/S linkers (Fig. 1B) (Davey et al., 2017). To shed additional light on the interactions with internal PDZbms, we further used a combinatorial peptide phage library of high complexity (Ilari et al., 2015). The libraries were used in selection against immobilized Shank1 PDZ. The peptide-coding regions of the binding-enriched phage pools were analyzed by next-generation sequencing (NGS). Consensus binding motifs were established for the enriched peptides using the SLiMfinder algorithm (Davey et al., 2010): x-T-x-(L/F)–COOH and -x-T-x-F-x, for the C-terminal and internal ProP-PD selections, respectively (Fig. 1C). High confidence sets of ligands were generated by removing low count sequences (total NGS count cut-off lower than 6), peptides that only occurred in one replicate, non-specific peptides occurring frequently in ProP-PD data sets, and peptides lacking the shared consensus motifs (Table S1).

The analysis of the C-terminal ProP-PD selection resulted in 53 C-terminal peptides that map to 65 proteins. Of these, 8 have previously been suggested as Shank1 binders based on the information in BioGRID and IntAct (Fig. 1D, Table S1) (Orchard et al., 2014; Oughtred et al., 2019). Notably, 9 of the C-terminal PDZbms are found in alternative isoforms of the main protein listed in UniProt, suggesting that alternative splicing may regulate PDZ-mediated interactions. Next, we aimed to narrow down the ligand set to interactions that are more likely to be of potential biological relevance. Of the 65 proteins, 4 proteins were flagged as not physiologically relevant as they are associated with localizations not compatible with interactions with Shank1 (i.e. extracellular or mitochondrial), leaving a set of 61 proteins for further analysis. We analyzed the gene ontology (GO) term enrichment among these proteins using the DAVID GO term tool (Huang et al., 2009) and found an enrichment of terms related to the biological function of Shank1, such as plasma membrane and transmembrane transport (Fig. 1E). By analyzing the overlap of GO terms with the bait, we further found that 39 of the hits share GO terms with Shank1 (e.g. synapse) that are unlikely to occur by chance ($p < 0.01$, Table S1).

For the internal PDZ ligand set, we generated a high-confidence set of 148 peptides from 137 proteins (Table S2). Among those, we noticed the $ACE2_{790\text{-}805}$ peptide that was identified as a Shank ligand in the internal ProP-PD selection, although the peptide is located at the extreme C-terminus of the protein. We then followed the same strategy as above to narrow down the set to ligands of higher potential biological relevance. 28 of the proteins were flagged as not physiologically relevant as they are secreted (Table S2). A GO term enrichment revealed that the set of interactors with internal PDZbms was enriched in proteins with GO terms related to the biological function of Shank1, such as positive regulation of neurological function (Fig. 1E). Indeed, 72 of the proteins with internal PDZbms share GO terms with Shank1 that are unlikely to occur by chance (e.g. neuron projection, synapse; $p < 0.01$) (Table S2). In comparison with our previous study (Davey et al., 2017), the repeated screens validated most of the previously reported interactions, and more than doubled the number of internal PDZbm instances found in ligands that share GO terms with Shank1. We visualized high-confidence ligands that shared GO terms with Shank1 PDZ using Cytoscape (Fig. 1F). This network includes interactions among identified ligands based on data from curated databases and also highlights validations discussed later.

For the combinatorial phage selection, we retrieved 160 ligands with a shared x-T-x-F-x motif and more than 5 NGS counts (Table S3). The consensus motif was essentially identical to the motif generated using the internal ProP-PD library (Fig. 1C). We found a preference for T at the p-2 position for both the C-terminal and the internal PDZbms. A notable difference between the internal and the C-terminal ligands (Fig. 1C) was the apparent strict requirement of an F in the p0 position of internal PDZbms.

2.2. Shank1 PDZ has generally higher affinities for C-terminal peptides

Having defined the consensus motifs and a filtered set of high-confidence ligands, we next explored the affinities of Shank1 PDZ for binding to C-terminal versus internal PDZbms. To this end, we selected a set of C-terminal peptides and a set of internal Shank1-binding peptides and determined the affinities of their interactions using microscale thermophoresis (MST). The K_d values as determined by MST were in the order of 0.1–20 μM (Table 1 and Fig. 2A and B), with the C-terminal ligands generally binding Shank1 PDZ with higher affinity. For the internal ligands of $MTOR_{55\text{-}70}$ and $DEPTOR_{258\text{-}273}$, we were unable to determine reliable K_d values using MST due to technical limitations of the method. Instead, we determined the K_d values of these interactions using fluorescence polarization (FP) to be 84 μM and 297 μM for $MTOR_{55\text{-}70}$ and $DEPTOR_{258\text{-}273}$, respectively (SI Figure S1). Notably, the internal-PDZbm containing peptides identified from the combinatorial phage library had similar affinity as those identified from the ProP-PD library,

Table 1
Overview of K_d values of Shank1 PDZ and C-terminal and internal PDZbms as determined by MST and FP.

Protein	Peptide	K_d (μM)
C-terminal ligands		
$DHRS2_{271-280}$	IAVAGYSTRL-COO^-	0.15 ± 0.01[a]
$TBC1D10C_{437-446}$	GSTSFLDTRF- COO^-	0.25 ± 0.02[a]
$SLC30A10_{476-485}$	DQCYVNRTHF- COO^-	0.48 ± 0.05[a]
$ARHGEF7_{795-803}$	DPAWDETNL- COO^-	0.79 ± 0.06[a]
$ANKS1B_{1239-1248}$	INTKYETTIF- COO^-	4.8 ± 0.8[a]
Internal ligands		
$ELFN1_{579-594}$	ESTSFQGVKSGPVSVA	1.6 ± 0.1[a]
$ARAP3_{1414-1429}$	FPELIQDTSTSFSTTR	3.0 ± 0.3[a]
$ATG13_{251-266}$	VCTTSFSTSPPSQLSS	3.8 ± 0.3[a]
$RIMS1_{1351-1366}$	SRTSSASRLSSTSFMS	5.5 ± 0.3[a]
$NRG1_{322-337}$	HIVEREAETSFSTSHY	13.5 ± 0.6[a]
$KCNMA1_{741-756}$	LSSVSVNDASTSFRAF	17 ± 1[a]
$RICTOR_{1153-1168}$	VQKTLQLETSFMGNKH	21 ± 2[a]
$MTOR_{55-70}$	MSQEESTRFYDQLNHH	84 ± 4[b]
$DEPTOR_{258-273}$	STSFMSVSPSKEIKIV	297 ± 16[b]
Predicted internal ligands		
$EXOC3_{2-17}$	MQCEDSTSFFTMKETD	3.4 ± 0.3[a]
$MTOR_{310-325}$	PRHITPFTSFQAVQPQ	N.B[c]
Ligands from combinatorial peptide phage display		
Comb Top 3	TSQVMENILSTTFQHE	6.4 ± 0.3[a]
Comb Top 2	QRIEQQWHTQTTSFDV	18 ± 1[a]

Data was obtained from at least three independent titrations and using different batches of purified protein.
[a] Determined through MST.
[b] Determined through FP.
[c] N.B.: Not Binding.

suggesting that this is an affinity limitation imposed by the binding mode, and not the limited search space of the ProP-PD library (Fig. 2C). We further tested the binding of two additional x-T-x-F-x containing peptides, $EXOC3_{2-17}$ and $MTOR_{310-325}$, that we predicted to be Shank1 binders based on the presence of the consensus motif. We successfully confirmed an interaction with $EXOC3_{2-17}$ but not with $MTOR_{310-325}$, suggesting that the context of the motif determines if it can bind to the domain or not.

2.3. Mutational analysis of the internal PDZbm of ARAP3

Using $ARAP3_{1414-1429}$ as a model peptide, we tested if exposing the internal PDZbm would affect the affinity of this peptide. We found that a C-terminally truncated ARAP3 bound Shank1 PDZ about 2.5 times more tightly, suggesting that additional interactions with the free carboxylate contributed to the interaction, or alternatively that steric hindrance between residues downstream of the internal PDZbm and the Shank1 PDZ domain weakened the interaction of the internal peptide (Fig. 3A and B). We further probed the importance of the core residues of the x-T-x-F-x motif and made conservative point mutations, replacing T with S, or F with L. Both mutations abrogated the interaction with the Shank1 PDZ. These results thus confirmed a dependency on an F at the p0 position for internal ligands and supported that there is a preference for a T over S at the p-2 position. To test the importance of the residue following the p0 position, we further mutated the p+1 S in $ARAP3_{1414-1429}$ to G. This conservative mutation resulted in a substantial loss of binding affinity, thus further demonstrating that the context of the motif is important.

2.4. Structural analysis of the Shank1-ARAP3 complex

In order to elucidate the molecular basis of ARAP3 binding to the PDZ domain of Shank1, we determined the crystal structure of a fusion protein of the Shank1 PDZ domain with a C-terminally attached ARAP3-derived peptide, at a resolution of 2.0 Å (Fig. 4 and Table S4). The crystals used for structure determination belonged to the hexagonal space group $P6_122$ with two molecules in the asymmetric unit (chains A and B in Fig. 4B). The biological dimers of those two molecules are produced through the crystallographic 2-fold symmetry axes (Fig. 4C). The overall fold of the Shank1 PDZ domain was essentially the same as seen in previously published structures and consists of a twisted five-

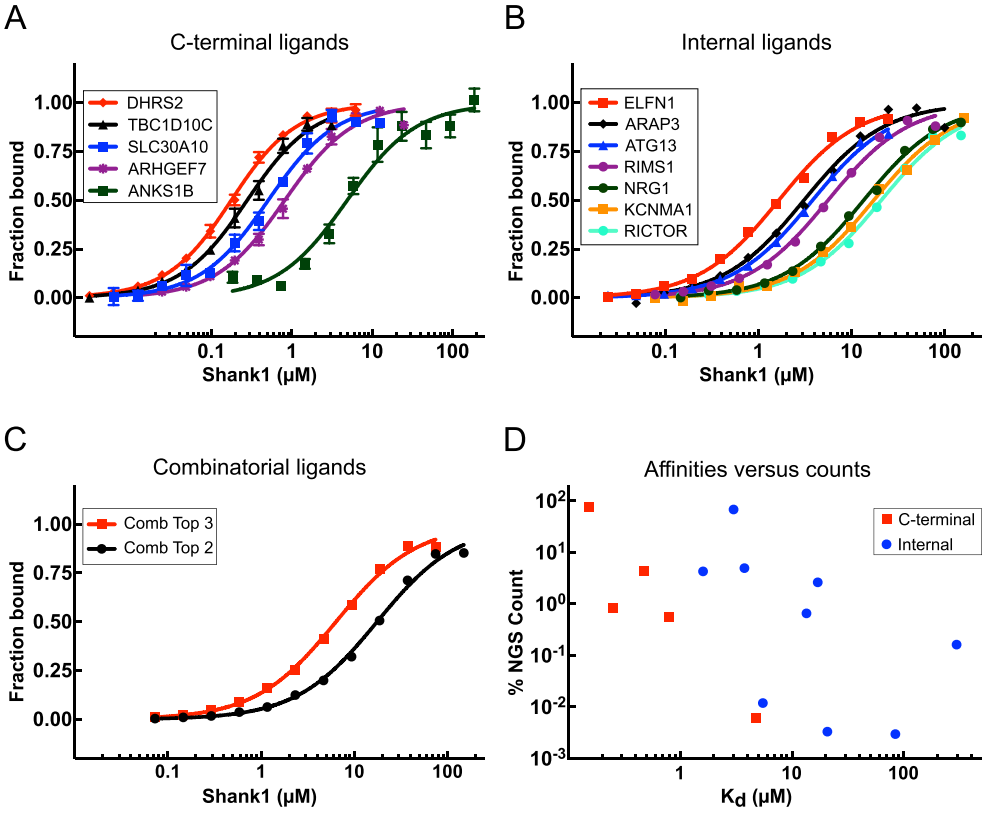

Fig. 2. Affinities of C-terminal and internal ligands for Shank1 PDZ as determined by MST using FITC-labeled synthetic peptides. The affinities of Shank1 PDZ for C-terminal PDZbms (A) are generally higher than the affinities for internal PDZbms (B and C). (D) Correlation between NGS counts and K_d values. For the C-terminal ligands there is a clear correlation, but it is less pronounced for the internal PDZbms. Data was obtained from averaging at least three independent titration experiments and using different batches of purified protein.

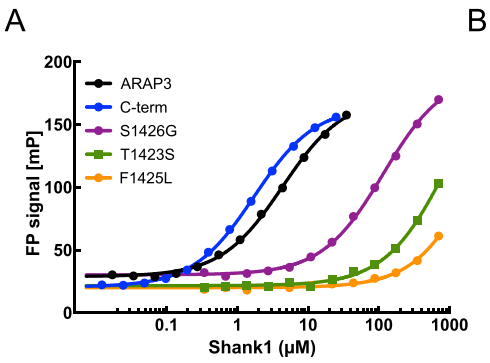

Peptide	Sequence	K_d (μM)
ARAP3	FPELIQDTSTSFSTTR	4.3 ± 0.2
C-term	FPELIQDTSTSF-coo	1.73 ± 0.03
S1426G	FPELIQDTSTSFGTTR	116 ± 4
T1423S	FPELIQDTSSSFSTTR	N.D.
F1425L	FPELIQDTSTSLSTTR	N.D.

Fig. 3. Mutational and truncation analysis of the internal PDZbm of ARAP3. (A) Affinity determination between Shank1 PDZ and $ARAP3_{1414-1429}$ and its variants as determined by FP. The mutational analysis confirmed the importance of key residues of the x-T-x-F-x motif and a serine at the p+1 position. (B) Summary of K_d values. Data presented here as means ± S.D. were obtained from averaging at least three independent titration experiments and using different batches of purified protein.

stranded antiparallel β-sheet and two α-helices (αA and αB). The model of chain B comprised residues 650–682 and 689–787, including the full linker region and the $ARAP3_{1414-1429}$ peptide bar the C-terminal arginine. Chain A was less well defined in certain regions. In addition to the partial disorder in the loop between β-strands 2 and 3 of the PDZ domain, the linker region was also disordered, and the last three residues of the $ARAP3_{1414-1429}$ peptide could not be modeled. Numbers in the following refer to the interaction of the C-terminal peptide in chain B with the PDZ domain of chain A. The ARAP3-derived sequence adopts a β-strand conformation and binds to a neighboring PDZ domain, where it is sandwiched between the αB helix and the second β-strand, thereby extending the central β-sheet of the PDZ domain. Essentially the same interaction pattern is seen for the ARAP3 peptide of chain A.

In addition to numerous main-chain hydrogen bonds through formation of an intermolecular β-sheet, the ARAP3-derived peptide formed a series of specific side-chain interactions with the PDZ domain (Fig. 4D). T782 at the p-2 position of the x-T-x-F-x consensus motif (T1423 in ARAP3) forms a strong hydrogen bond with the side chain of H735 (distance = 2.6 Å). Its Cγ-atom packs against the side chain of V739, which explains the preference for a threonine over a serine at this position. The crucial aromatic residue in this motif, F784, at the p0 position (F1425 in ARAP3) binds to a unique pocket, making extensive hydrophobic interactions with the side chains of F674, F676 and L678, as well as V739, I742 and the aliphatic part of the R743 side chain on the αB helix. The importance of these hydrophobic packing interactions is highlighted by the drastically reduced affinity of an ARAP3-dervived peptide with a hydrophobic large-to-small substitution (F to L) at this position (Fig. 3). The two amino acids directly after the consensus motif are also involved in specific interactions with the PDZ domain: S785 forms a hydrogen bond with the side-chain carboxylate of D706, and the T786 hydroxyl group is hydrogen-bonded to the main-chain nitrogen of G673. The total binding interface is 705 $Å^2$, calculated using the PISA server (Krissinel and Henrick, 2007).

A comparison of the biological PDZ dimers in our structure with those in the structures with the β-PIX (ARHGEF7) coiled-coil domain (PDB entry 3L4F (Im et al., 2010)) and the derived DETNL-COOH pentapeptide (PDB entry 3QJM (Lee et al., 2011)) revealed an intriguing fluidity of the dimer interface region, and hence the relative orientation of the subunits, as a result of different binding partners and crystallographic environment (SI Figure S2). There are displacements of the αB helix of up to 20 Å. Such a fluid interface may, therefore, facilitate Shank1's scaffolding functions, enabling its PDZ domain to effectively interact with multiple binding partners within complex interaction networks.

2.5. Comparison of the Shank1-ARAP3 binding mode with other PDZ-peptide complexes

The binding mode of the internal ARAP3 peptide mimics that of the C-terminal PDZ binding motif of β-PIX (Lee et al., 2011) as shown in the superimposition in Fig. 4D. Both oxygens of the C-terminal carboxylate in the Shank1-β-PIX complex form hydrogen bonds with the main-chain NH groups of F674 and G675. In the Shank1-ARAP3 complex, the main-chain oxygen of F784 interacts also with F674 and G675. With a total binding interface area of 590 $Å^2$, the Shank1-β-PIX interface in PDB entry 3L4F was almost 20% smaller than that of the Shank1-ARAP3 interface described above. Yet, the affinity of the β-PIX-derived peptide (Table 1) was more than three times higher than that of the ARAP3 peptide. Interestingly, the truncated ARAP3 peptide without additional residues after the consensus PDZ-binding motif also showed a 2.5-fold increase in affinity. For a C-terminal binding motif, the charged hydrogen bonds through direct interaction of the C-terminal carboxylate, therefore, seem to overcompensate for the loss of binding interface and result in stronger binding. This observation is also reflected by the trend in Table 1, where C-terminal peptides generally had a higher affinity than internal peptides.

A few other structures of PDZ domains bound to internal peptides have been reported. In two complexes where the PDZ domains have a conserved binding pocket (Fig. 5A), the signature x-T-x-F-x motif adopted essentially the same binding mode as observed in our Shank1 complex, but there were differences in the interaction of flanking residues for: the first PDZ domain of Scribble bound to an internal peptide derived from the Rho-specific guanine exchange factor SGEF (PDB entry 6MYE (Awadia et al., 2019)) and α-syntrophin PDZ domain bound to an nNOS-derived peptide (PDB entry 1QAV (Hillier et al., 1999)).

In the complex of the cell polarity protein Par6 PDZ domain with a Pals1-derived peptide (PDB entry 1X8S (Penkert et al., 2004)), however, the T-x-F motif is replaced by M-A-V, and the binding mode of the peptide to PDZ varies slightly (Fig. 5B). The peptide backbone protrudes deeper into the pocket in the PDZ domain, enabling the shorter valine at the p0 position to mimic the phenylalanine-mediated interaction in the Shank1 complex. The histidine residue that forms a hydrogen bond with the threonine hydroxyl at the p-2 position in Shank1 (and the other two above-mentioned PDZ domains) is replaced by a leucine (L231). This variation results in a hydrophobic sub-pocket to accommodate the methionine side chain, which explains why the Par6 PDZ also binds peptides with a hydrophobic residue at p-2. In addition, the binding mode of the Pals1-derived internal peptide is stabilized by salt bridges at positions p1, p-3 and p-4 (Fig. 5B). In the recently published complex of the C-terminal PDZ domain of Whirlin with a Taperin-derived peptide (PDB entry 6Y9Q (Zhu et al., 2020)), the bound internal peptide also contains a smaller hydrophobic residue in the p0 position, in this case an isoleucine. An interesting feature of this structure compared with the Par6-Pals1 complex (and also the Shank1-ARAP3 complex) is the different exit of the peptide from the binding pocket in the direction of the αB helix. The Pals1 and Taperin peptides both contain an aspartate at the p1 position. This aspartate forms a salt bridge with a lysine at the periphery of the binding pocket in the Par6 complex. In the Whirlin--Taperin complex, however, the aspartate side chain folds back into the pocket and interacts with two backbone amines of the

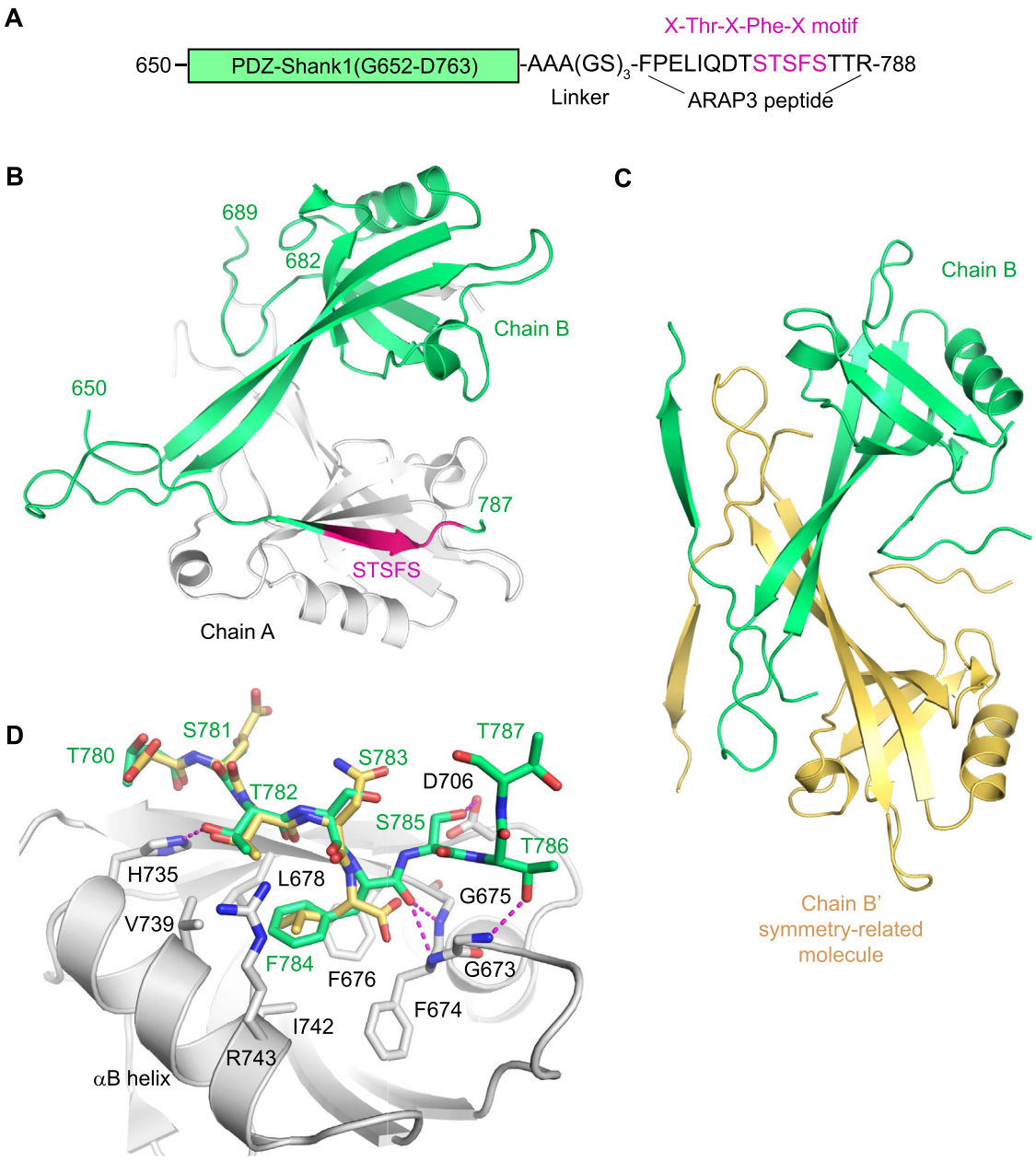

Fig. 4. Crystal structure of the Shank1 PDZ-ARAP3 fusion protein. (A) Design of the Shank1 PDZ-ARAP3 fusion protein. Residues 773-788 of the fusion protein correspond to ARAP3 residues 1414-1429. (B) Asymmetric unit of the crystal structure containing two chains of the fusion protein shown as cartoon representation. (C) Biological PDZ dimer along the crystallographic 2-fold symmetry axis. (D) Binding mode of the ARAP3-derived peptide (green stick model; chain B) to the PDZ domain of chain A (gray cartoon and stick model). Selected hydrogen bonds between ARAP3 and the PDZ domain are highlighted by magenta broken lines. The binding mode of the C-terminal pentapeptide of βPIX in PDB entry 3QJM (Lee et al., 2011) is shown as yellow stick model. The superposition is based on the PDZ domains in both structures. The PDZ domain of the latter structure was omitted for clarity.

carboxylate-binding loop (the conserved glycine and the preceding leucine residue), reminiscent of the binding mode of the carboxy terminus of C-terminal peptides.

2.6. Validation of interactions in the context of full-length proteins

We next wanted to establish if ligands with C-terminal and internal PDZbms also interacted with Shank1 PDZ in the context of full-length proteins, where binding motifs may be conformationally constrained or occluded. We selected three potential interaction partners with C-terminal PDZbms (TBC1D10C, SLC30A10, ANKS1B) and five examples with internal PDZbms (ELFN1, ARAP3, NRG1, ATG13 and DEPTOR) for validation by pull-down experiments. Among these proteins, ARAP3 and TBC1D10C are both GTPase-activating proteins, of which ARAP3 is involved in cytoskeleton remodeling (Myers and Casanova, 2008) and TBC1D10C inhibits Calcineurin (Parra and Rothermel, 2017). NRG1, ELFN1, SLC30A10 and ANKS1B were selected based on their involvement in different processes related to CNS development and functions and their localization in neuronal cells. ATG13 is involved in autophagy-related TOR signaling with other proteins, including MTOR, DEPTOR and RICTOR (Jung et al., 2010).

Tagged full-length ligand proteins were transiently expressed in HEK293 cells for 48 h and pull-down experiments were performed by either pulling with GST-tagged Shank1 PDZ and blotting against the tag

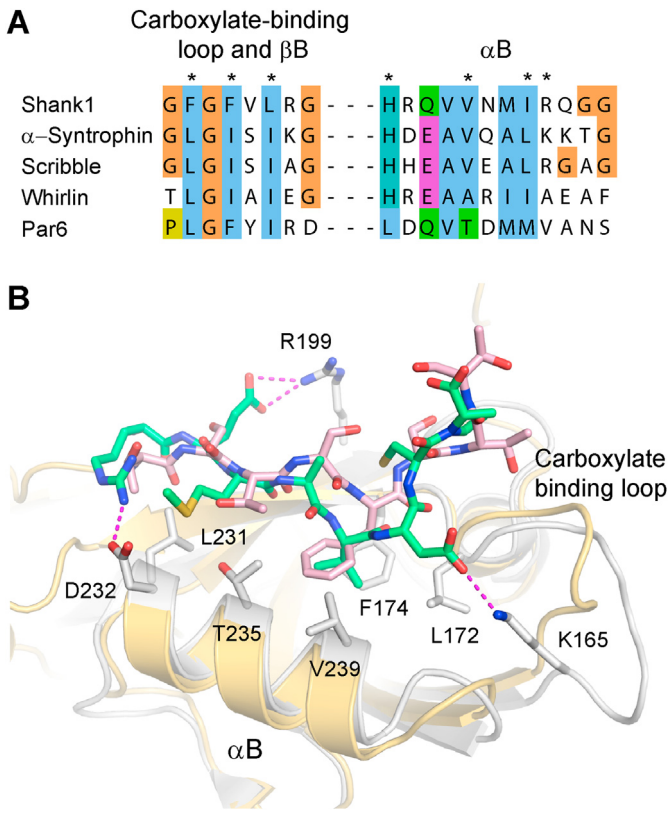

Fig. 5. Binding of internal PDZbms to different PDZ domains. (A) Sequence alignment of the peptide-binding pocket in the PDZ domain of human Shank1 (UniProt Q9Y566), Scribble (UniProt Q14160; first PDZ domain), α-Syntrophin (UniProt Q13424), Whirlin (UniProt Q9P202; C-terminal PDZ domain), and Par6 (UniProt Q9NPB6). Amino acids are colored according to type and conservation (Clustal X color scheme). Residues that form key side-chain interactions in the Shank1-peptide complex are marked with an asterisk. (B) Superposition of the binding mode of the internal peptide in *Drosophila* Par6 (PDB code 1X8S) and our Shank1-ARAP3 fusion protein. PDZ domains are shown as cartoon models in gray (Par6) and yellow (Shank1), bound peptides as stick models in green (Par6 complex) and pink (Shank1 complex). Selected side chains in the binding pocket of the Par6 domain are shown as gray stick models, and salt bridges between the PDZ domain and the peptide are highlighted (magenta broken lines). All binding-pocket residues are conserved between human and *Drosophila* Par6. Side chains of Shank1 were omitted for clarity.

of the ligand protein, or vice versa (Fig. 6). Interactions were confirmed for all proteins except DEPTOR, which according to the affinity data only interacted with Shank1 PDZ with low affinity. Mutations of the PDZbms in the context of the full-length proteins abrogated the interactions, thus confirming that the interactions rely on the identified PDZbms.

3. Concluding remarks

In this study, we performed an integrated analysis of the interactions of Shank1 PDZ domain with C-terminal and internal binding sites. We refined the consensus binding sequence for the two different types of PDZbms and found a multitude of potential novel interaction partners. The Shank1 PDZ domain bound both types of ligands with low micromolar affinities, and without structural alterations of the PDZ domain. The flexible peptide motifs with internal PDZbms dock the key residues x-T-x-F-x into the canonical binding groove, exclusively requiring an F at the p0 position. Importantly, we confirmed that the interactions with the internal PDZbms can occur also in the context of the full-length proteins. The study thus expands the interactome of Shank1 and provides detailed information on the binding interfaces and sequence requirements. This information might also be valuable for understanding the molecular basis of how mutations of Shank proteins and their ligands associate with conditions such as autism spectrum disorder and schizophrenia. Taken together, our data has shed new light on the interaction space formed by PDZ domains and proteins with internal PDZbms, and should inspire future studies on this largely unexplored area of the human interactome.

4. Methods and materials

4.1. Constructs, cloning and mutagenesis

The construct of human Shank1 PDZ (652–765) in pHH0103 has been reported before (Davey et al., 2017). pEGFP-ARAP3 was a gift from Dr. Sonja Vermeren (Addgene plasmid #39484). RV-Syn-Dio-YFP_2a_ELFN1 was a gift from Dr. Oscar Marin (Addgene plasmid #98177). The ELFN1 gene was PCR amplified and cloned into CMV10 vector using BamHI and EcoRI sites. myc-Rictor was a gift from Dr. David Sabatini (Addgene plasmid #11367). npLenti6/V5-hANKS1B was a gift from Dr. Andreas Fischer (Herberich et al., 2015). The gene encoding full-length ANKS1B was PCR amplified and cloned into CMV10 vector using NotI and BglII sites. NRG1-FLAG was kindly provided by Dr. Andreas Herrlich (Parra et al., 2015). FLAG-Myc-Carabin was a gift from Dr. Fan Pan (Pan et al., 2007). SLC30A10-FLAG was a gift from Dr. Somshuvra Mukhopadhyay (Zogzas et al., 2016). All cloned genes were sequenced to confirm identity. QuickChange based site-directed mutagenesis protocol was adopted to introduce mutations of the PDZbms. For generating the Shank1 PDZ and ARAP3 peptide fused construct, Shank1 PDZ was PCR amplified with extended annealing oligos to introduce a linker (coding for 3 GS tandem repeats) and the DNA sequence of ARAP3 peptide (UniProt Q8WWN8: residues 1414–1429). This amplicon was subsequently cloned into pETM-11 using NcoI and XhoI sites. The sequences were verified by Sanger sequencing.

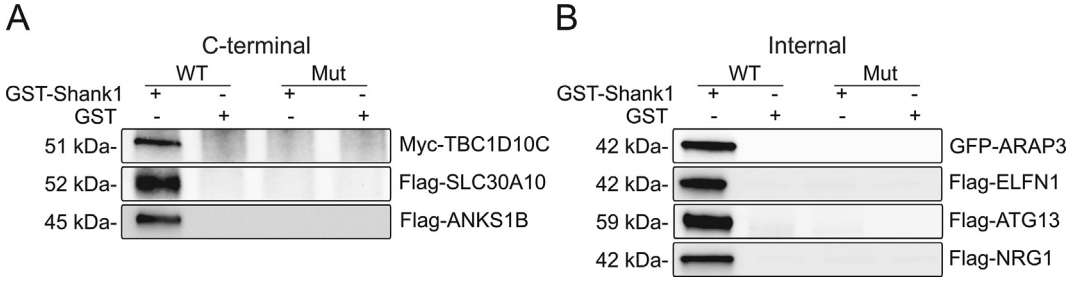

Fig. 6. Pull-down validations of interactions with full-length PDZbm containing proteins. (A) Lysates from cells expressing proteins with C-terminal ligands were incubated with GST-Shank1 PDZ or GST (as negative control) and immunoprecipitated using Glutathione Magnetic Agarose Beads. Samples were separated using SDS-PAGE and evaluated by immunoblotting using Anti-FLAG (SLC30A10 and ANKS1B) and MYC (TBC1D10C) antibodies. (B) Lysates from cells expressing ligands with internal PDZbms were similarly incubated with GST-Shank1 PDZ or GST and immunoprecipitated using either of the magnetic beads: magnetic GFP-Trap, Glutathione Magnetic Agarose Beads and Anti-FLAG M2 Magnetic Beads. Samples were immunoblotted using anti-GST against GST-tagged Shank1 PDZ (ELFN1, ARAP3 and NRG1) or anti-FLAG (ATG13) antibodies.

4.2. Protein expression and purification

GST-tagged Shank1 PDZ was expressed in *E. coli* BL21(DE3) for phage display selections and affinity measurements starting from the pHH0103 vector containing the gene encoding Shank1 PDZ. Protein was expressed by growing bacteria in 2x YT media at 37 °C until OD_{600} reached 0.6–0.8 and then induced with 0.3 mM isopropyl β-d-1-thiogalactopyranoside (IPTG) at 18 °C for 16 h. Cells were harvested by centrifuging at 7000 xg for 10 min. Pellets were resuspended in lysis buffer: PBS (137 mM NaCl, 2.7 mM KCl, 10 mM Na_2HPO_4, 1.8 mM KH_2PO_4, pH 7.4) containing DNase I, lysozyme, protease inhibitor cocktail, 1% Triton X-100 and 2 mM ß-mercaptoethanol pH 7.4 for 30 min at 4 °C with shaking. Cell debris was separated by centrifuging at 25,000 xg for 45 min. Lysate was incubated with glutathione (GSH) sepharose resin (GE) for 1–2 h at 4 °C with shaking. Contaminant proteins were washed away with PBS. Protein was eluted using 10 mM reduced GSH in PBS (pH 8.0). The GST-tag was removed before affinity measurements by cleaving with HRV 3C protease overnight while dialyzing the protein in MST experimental buffer (PBS pH 7.4, 10 mM $MgCl_2$, 0.05% Tween-20 and 1 mM DTT). The cleaved GST-tag was removed using reverse Ni-IMAC.

For crystallization, we used a pETM-11-based expression vector encoding a fusion protein with an N-terminal 6xHis tag, followed by a TEV protease cleavage site, the PDZ domain of Shank1 (residues 652–765), followed by a glycine and serine-rich linker (3 GS repeats) and the internal PDZ binding motif of ARAP3 (residues 1414–1429). The recombinant fusion protein was expressed in *E. coli* Rosetta (DE3). Cells harboring the expression vector were grown in TB medium at 37 °C until an OD_{600} of 1.5–1.8 was reached. The temperature was lowered to 18 °C, and protein expression was induced by adding 0.5 mM IPTG. Cells were harvested the next day. After breaking the cells by sonication, the protein was purified using affinity chromatography on Ni-NTA agarose, followed by TEV protease cleavage overnight to remove the 6xHis tag. After a reverse IMAC, the protein was purified further by gel filtration on a Superdex75 16/600 column (GE Healthcare) in 10 mM HEPES buffer, pH 8.0, 150 mM NaCl, 5% (v/v) glycerol and 0.5 mM TCEP. The pooled fractions from the gel filtration were concentrated to 15 mg/ml, flash frozen in liquid nitrogen and stored at −80 °C.

4.3. ProP-PD selections

Phage selections were performed for 4 rounds following established protocols and using previously described libraries (Ivarsson et al., 2014). Briefly, 25 μg of the GST-tagged Shank1 PDZ and negative control (GST) were immobilized separately to a 96-well Maxisorp plate overnight at 4 °C with shaking. Unbound proteins were removed, and wells were blocked using 0.5% BSA for an hour at 4 °C with shaking. Phage library containing 10^{11} CFU per well was precipitated using 1/5th volume of PEG/NaCl and centrifugation at 10,000xg for 10 min. Selected and amplified phages from each day were similarly precipitated. Prior to introducing phages, control and Shank1 PDZ-coated wells were washed 4 times using PBS containing 0.05% Tween-20 (PBST). 100 μl of phage solution was added to control wells and incubated for 1 h at 4 °C with shaking to remove non-specific phages. They were later transferred to Shank1-coated wells and incubated for 2 h at 4 °C with shaking. Unbound phages were removed, and wells were washed once again like before. Bound phages were eluted using 100 μl of mid log-phase *E.coli* OmniMax culture by incubation at 37 °C for 30 min. M13KO7 helper phages (10^{11} pfu/ml) were added to infect bacteria and incubated at 37 °C for 45 min. This eluent was then transferred to 10 ml of 2xYT medium containing kanamycin, carbenicillin and 0.3 mM IPTG and incubated overnight at 37 °C.

Phage pool ELISA was performed to determine the selection success. Shank1 PDZ (10 μg) and GST control were immobilized overnight. The following day, wells were blocked with BSA. 100 μl of phage solution was added to each well and incubated for 1 h at 4 °C with shaking. Unbound phages were removed by washing 5 times using PBST, and anti-M13 coat HR-conjugate antibody was added (1:5000 dilution). Unbound antibody was washed as before, and TMB substrate was added until the blue color developed. Reaction was stopped using 0.6 M H_2SO_4. Absorbance from each well was recorded at 450 nm. Peptide-coding regions of binding-enriched phage pools were barcoded and amplified by PCR. These DNA pools were sequenced using NGS, and results were analyzed as described elsewhere (Ivarsson et al., 2014).

4.4. MST

10-mer or 16-mer unlabeled and FITC-labeled synthetic peptides were obtained with >95% purity (GeneCust). Peptides were dissolved in minimal amount of DMSO and later diluted to working concentration (100 nM) using MST experimental buffer. 10 μl of 10–200 μM protein was serially diluted using 10 μl of MST experimental buffer in a non-binding 384 microwell plate (Greiner Bio-One). 10 μl of labeled peptide was mixed with the protein solutions and incubated for 5 min at room temperature. Standard capillaries (Nanotemper) were used to analyze the sample in a Monolith NT.Automated machine (Nanotemper) using blue filter and 20 or 40 MST power. The measurements were replicated to achieve statistically significant data. Results were analyzed with MO.Affinity Analysis V2.3 software. The data was fitted using a standard quadratic equation for equilibrium binding (Chi et al., 2008), with the peptide concentration fixed to 50 nM.

4.5. FP assay

To obtain saturation curves, 25 μl of 10 nM FITC-labeled synthetic peptide was added and mixed to 25 μl of titrated protein solution in FP buffer (PBS pH 7.4, 10 mM $MgCl_2$, 0.05% Tween-20 and 1 mM DTT). FP was measured using SpectraMax iD5 (Molecular Devices) in triplicates. The data was fitted using a standard quadratic equation for equilibrium binding (Chi et al., 2008), with the peptide concentration fixed to 5 nM. Independent replicates were performed to obtain statistically significant data.

4.6. Protein crystallization and structure determination

Crystals of the Shank1 PDZ-ARAP3 fusion protein were grown at 20 °C via the sitting drop vapor diffusion technique using a Mosquito® crystallization robot (TTP Labtech, Royston UK) and SWISSCI 3-lens crystallization plates. 100 nl of protein solution (15 mg/ml fusion protein in 10 mM HEPES buffer, pH 8.0, 150 mM NaCl, 5% (v/v) glycerol and 0.5 mM TCEP) were mixed with 100 nl reservoir buffer (16% (w/v) polyethylene glycol 3350 and 0.2 M ammonium citrate) above a reservoir volume of 20 μl. Rod-shaped crystals appeared after a couple of weeks. For data collection, the crystals were cryoprotected with mother liquor supplemented with 25% polyethylene glycol 400 and flash-frozen in liquid nitrogen. X-ray data sets were collected at 100 K at beamline X06SA of the Swiss Light Source, Villigen, Switzerland. The diffraction data were integrated with the program XDS (Kabsch, 2010) and scaled with AIMLESS (Evans, 2011), which is implemented in the CCP4 package (Winn et al., 2011). The structure was then solved by molecular replacement with PHASER (McCoy et al., 2007) using PDB entry 1Q3O as a search model and subsequently refined using iterative cycles of manual model building in COOT (Emsley et al., 2010) and refinement in PHENIX (Adams et al., 2010). Data collection and refinement statistics are listed in Table S4. Structural figures were prepared using PyMOL (www.pymol.org).

4.7. Cell culture and immunoprecipitation

HEK293 cells (Sigma:85120602) were cultured in treated T-25 flasks or 6-well plates using DMEM medium (Gibco™) supplemented with 10% FBS and 1x NEAA (Gibco™) at 37 °C and 5% CO_2. For pull downs, cells were transfected with 3 μg of target plasmid using Fugene® HD and

grown in complete medium for about 48–60 h post-transfection. Cells were washed with ice-cold washing buffer (PBS, Halt™ Protease Inhibitor Cocktail, pH 7.4), followed by incubation with lysis buffer (50 mM Tris-HCl, pH 7.4, 150 mM NaCl, 10 mM sodium pyrophosphate, 10 mM sodium orthovanadate, 10 mM sodium fluoride, 1x cOmpleate™ EDTA-free protease inhibitor tablet and 0.5% Nonidet P-40). Cell debris was removed by centrifugation, and sample protein was quantified using BCA Protein Assay (Pierce™). Lysates with 0.5 mg total protein content were mixed with target beads and rolled overnight at 4 °C. Glutathione Magnetic Agarose Beads (Pierce™), magnetic GFP-Trap® (Chromotek) and Anti-FLAG® M2 Magnetic Beads (Sigma) were used for pulling down respective tagged-proteins according to the manufacturer's recommendation. Beads with pulled-down proteins were washed three times with lysis buffer and later boiled with SDS sample buffer. Samples were electrophoresed and transferred to a nitrocellulose membrane. Membranes were blocked with 5% nonfat dried milk in TBST for 1 h. Membranes were immunoblotted with anti-FLAG (sigma), anti-GFP (ab6556), anti-HA (Sigma) anti-GST (Sigma) and anti-Myc (ab9106) antibodies followed by HRP-conjugated anti-rabbit secondary antibodies (GE). Signals were developed using Amersham ECL™ western blotting detection reagent (GE) and recorded with ChemiDoc™ Imaging system (Bio-Rad).

Author contributions

MA and SL performed ProP-PD selections. MA performed biophysical affinity measurements, pull downs and bioinformatic analysis. MMM and ACJ solved the crystal structure. All authors analyzed data. MA, ACJ, SK and YI wrote the manuscript, which has been approved by all authors.

Data availability

Atomic coordinates and structure factor amplitudes of the Shank1 PDZ ARAP3 fusion protein have been deposited in the Protein Data Bank (www.rcsb.org); PDB accession code 7A9B.

Declaration of competing interest

The authors declare that they have no known competing financial interests or personal relationships that could have appeared to influence the work reported in this paper.

Acknowledgements

This study was funded in part by grants from the Swedish research council (2016–04965 to Y. I.) and by the European Union's Horizon 2020 Research and Innovation Program under Marie Sklodowska-Curie Grant Agreement 675341 (to Y. I. and S. K.). A.C.J. is supported by German Research Foundation (DFG) grant JO 1473/1-3. SK and ACJ are grateful for support by the SGC, a registered charity (no. 1097737) that receives funds from AbbVie, Bayer AG, Boehringer Ingelheim, Canada Foundation for Innovation, Eshelman Institute for Innovation, Genentech, Genome Canada through Ontario Genomics Institute [OGI-196], EU/EFPIA/OICR/McGill/KTH/Diamond, Innovative Medicines Initiative 2 Joint Undertaking [EUbOPEN grant 875510], Janssen, Merck KGaA (aka EMD in Canada and US), Merck & Co (aka MSD outside Canada and US), Pfizer, São Paulo Research Foundation-FAPESP, Takeda and Wellcome [106169/ZZ14/Z]. Data collection at the Swiss Light Source was supported by funding from the European Union's Horizon 2020 research and innovation program grant agreement number 730872, project CALIPSOplus. We thank the staff at beamline X06SA of the Swiss Light Source for assistance during data collection.

Access to the Monolith NT automated MST was provided by the SciLifeLab Drug Discovery and Development platform with initial technical guidance provided by Dr. Annette Roos. Sequencing was performed by the SNP&SEQ Technology Platform in Uppsala. The facility is part of the National Genomic Infrastructure (NGI) Sweden and Science for Life Laboratory. The SNP&SEQ Platform is also supported by the Swedish Research Council and the Knut and Alice Wallenberg Foundation. The authors acknowledge the kind support of Dr. Norman Davey and Dr. Izabella Krystkowiak related to annotation of peptide hits and generation of consensus motifs. The combinatorial peptide-phage display library was generously provided by Prof. Sachdev Sidhu.

Appendix A. Supplementary data

Supplementary data to this article can be found online at https://doi.org/10.1016/j.crstbi.2021.01.001.

References

Adams, P.D., Afonine, P.V., Bunkoczi, G., Chen, V.B., Davis, I.W., Echols, N., et al., 2010. PHENIX: a comprehensive Python-based system for macromolecular structure solution. Acta Crystallogr. Sect. D Biol. Crystallogr. 66, 213–221.

Awadia, S., Huq, F., Arnold, T.R., Goicoechea, S.M., Sun, Y.J., Hou, T., et al., 2019. SGEF forms a complex with Scribble and Dlg1 and regulates epithelial junctions and contractility. J. Cell Biol. 218, 2699–2725.

Chi, C.N., Elfstrom, L., Shi, Y., Snall, T., Engstrom, A., Jemth, P., 2008. Reassessing a sparse energetic network within a single protein domain. Proc. Natl. Acad. Sci. U.S.A. 105, 4679–4684.

Davey, N.E., Haslam, N.J., Shields, D.C., Edwards, R.J., 2010. SLiMFinder: a web server to find novel, significantly over-represented, short protein motifs. Nucleic Acids Res. 38, W534–W539.

Davey, N.E., Seo, M.H., Yadav, V.K., Jeon, J., Nim, S., Krystkowiak, I., et al., 2017. Discovery of short linear motif-mediated interactions through phage display of intrinsically disordered regions of the human proteome. FEBS J. 284, 485–498.

Egea-Jimenez, A.L., Gallardo, R., Garcia-Pino, A., Ivarsson, Y., Wawrzyniak, A.M., Kashyap, R., et al., 2016. Frizzled 7 and PIP2 binding by syntenin PDZ2 domain supports Frizzled 7 trafficking and signalling. Nat. Commun. 7, 12101.

Emsley, P., Lohkamp, B., Scott, W.G., Cowtan, K., 2010. Features and development of coot. Acta Crystallogr. Sect. D Biol. Crystallogr. 66, 486–501.

Ernst, A., Appleton, B.A., Ivarsson, Y., Zhang, Y., Gfeller, D., Wiesmann, C., et al., 2014. A structural portrait of the PDZ domain family. J. Mol. Biol. 426, 3509–3519.

Evans, P.R., 2011. An introduction to data reduction: space-group determination, scaling and intensity statistics. Acta Crystallogr. Sect. D Biol. Crystallogr. 67, 282–292.

Gallardo, R., Ivarsson, Y., Schymkowitz, J., Rousseau, F., Zimmermann, P., 2010. Structural diversity of PDZ-lipid interactions. Chembiochem : a European journal of chemical biology 11, 456–467.

Gogl, G., Biri-Kovacs, B., Durbesson, F., Jane, P., Nomine, Y., Kostmann, C., et al., 2019. Rewiring of RSK-PDZ interactome by linear motif phosphorylation. J. Mol. Biol. 431, 1234–1249.

Herberich, S.E., Klose, R., Moll, I., Yang, W.J., Wustehube-Lausch, J., Fischer, A., 2015. ANKS1B interacts with the cerebral cavernous malformation protein-1 and controls endothelial permeability but not sprouting angiogenesis. PloS One 10, e0145304.

Hillier, B.J., Christopherson, K.S., Prehoda, K.E., Bredt, D.S., Lim, W.A., 1999. Unexpected modes of PDZ domain scaffolding revealed by structure of nNOS-syntrophin complex. Science 284, 812–815.

Huang, da W., Sherman, B.T., Lempicki, R.A., 2009. Systematic and integrative analysis of large gene lists using DAVID bioinformatics resources. Nat. Protoc. 4, 44–57.

Ilari, A., Fiorillo, A., Poser, E., Lalioti, V.S., Sundell, G.N., Ivarsson, Y., et al., 2015. Structural basis of Sorcin-mediated calcium-dependent signal transduction. Sci. Rep. 5, 16828.

Im, Y.J., Kang, G.B., Lee, J.H., Park, K.R., Song, H.E, Kim, E., et al., 2010. Structural basis for asymmetric association of the betaPIX coiled coil and shank PDZ. J. Mol. Biol. 397, 457–466.

Im, Y.J., Lee, J.H., Park, S.H., Park, S.J., Rho, S.H., Kang, G.B., et al., 2003. Crystal structure of the Shank PDZ-ligand complex reveals a class I PDZ interaction and a novel PDZ-PDZ dimerization. J. Biol. Chem. 278, 48099–48104.

Ivarsson, Y., 2012. Plasticity of PDZ domains in ligand recognition and signaling. FEBS Lett. 586, 2638–2647.

Ivarsson, Y., Wawrzyniak, A.M., Kashyap, R., Polanowska, J., Betzi, S., Lembo, F., et al., 2013. Prevalence, specificity and determinants of lipid-interacting PDZ domains from an in-cell screen and in vitro binding experiments. PloS One 8, e54581.

Ivarsson, Y., Arnold, R., McLaughlin, M., Nim, S., Joshi, R., Ray, D., et al., 2014. Large-scale interaction profiling of PDZ domains through proteomic peptide-phage display using human and viral phage peptidomes. Proc. Natl. Acad. Sci. U.S.A. 111, 2542–2547.

Jung, C.H., Ro, S.H., Cao, J., Otto, N.M., Kim, D.H., 2010. mTOR regulation of autophagy. FEBS Lett. 584, 1287–1295.

Kabsch, W., 2010. Xds. Acta crystallographica Section D, Biological crystallography 66, 125–132.

Krissinel, E., Henrick, K., 2007. Inference of macromolecular assemblies from crystalline state. J. Mol. Biol. 372, 774–797.

Leblond, C.S., Nava, C., Polge, A., Gauthier, J., Huguet, G., Lumbroso, S., et al., 2014. Meta-analysis of SHANK mutations in autism spectrum disorders: a gradient of severity in cognitive impairments. PLoS Genet. 10, e1004580.

Lee, J.H., Park, H., Park, S.J., Kim, H.J., Eom, S.H., 2011. The structural flexibility of the shank1 PDZ domain is important for its binding to different ligands. Biochem. Biophys. Res. Commun. 407, 207–212.
Luck, K., Fournane, S., Kieffer, B., Masson, M., Nomine, Y., Trave, G., 2011. Putting into practice domain-linear motif interaction predictions for exploration of protein networks. PloS One 6, e25376.
McCoy, A.J., Grosse-Kunstleve, R.W., Adams, P.D., Winn, M.D., Storoni, L.C., Read, R.J., 2007. Phaser crystallographic software. J. Appl. Crystallogr. 40, 658–674.
Myers, K.R., Casanova, J.E., 2008. Regulation of actin cytoskeleton dynamics by Arf-family GTPases. Trends Cell Biol. 18, 184–192.
Orchard, S., Ammari, M., Aranda, B., Breuza, L., Briganti, L., Broackes-Carter, F., et al., 2014. The MIntAct project–IntAct as a common curation platform for 11 molecular interaction databases. Nucleic Acids Res. 42, D358–D363.
Oughtred, R., Stark, C., Breitkreutz, B.J., Rust, J., Boucher, L., Chang, C., et al., 2019. The BioGRID interaction database: 2019 update. Nucleic Acids Res. 47, D529–D541.
Pan, F., Sun, L., Kardian, D.B., Whartenby, K.A., Pardoll, D.M., Liu, J.O., 2007. Feedback inhibition of calcineurin and Ras by a dual inhibitory protein Carabin. Nature 445, 433–436.
Parra, V., Rothermel, B.A., 2017. Calcineurin signaling in the heart: the importance of time and place. J. Mol. Cell. Cardiol. 103, 121–136.
Parra, L.M., Hartmann, M., Schubach, S., Li, Y., Herrlich, P., Herrlich, A., 2015. Distinct intracellular domain substrate modifications selectively regulate ectodomain cleavage of NRG1 or CD44. Mol. Cell Biol. 35, 3381–3395.
Peca, J., Feliciano, C., Ting, J.T., Wang, W., Wells, M.F., Venkatraman, T.N., et al., 2011. Shank3 mutant mice display autistic-like behaviours and striatal dysfunction. Nature 472, 437–442.
Penkert, R.R., DiVittorio, H.M., Prehoda, K.E., 2004. Internal recognition through PDZ domain plasticity in the Par-6-Pals1 complex. Nat. Struct. Mol. Biol. 11, 1122–1127.
Soler, J., Fananas, L., Parellada, M., Krebs, M.O., Rouleau, G.A., Fatjo-Vilas, M., 2018. Genetic variability in scaffolding proteins and risk for schizophrenia and autism-spectrum disorders: a systematic review. J. Psychiatry Neurosci. 43, 223–244.
Songyang, Z., Fanning, A.S., Fu, C., Xu, J., Marfatia, S.M., Chishti, A.H., et al., 1997. Recognition of unique carboxyl-terminal motifs by distinct PDZ domains. Science 275, 73–77.
Stiffler, M.A., Chen, J.R., Grantcharova, V.P., Lei, Y., Fuchs, D., Allen, J.E., et al., 2007. PDZ domain binding selectivity is optimized across the mouse proteome. Science 317, 364–369.
Sundell, G.N., Arnold, R., Ali, M., Naksukpaiboon, P., Orts, J., Guntert, P., et al., 2018. Proteome-wide analysis of phospho-regulated PDZ domain interactions. Mol. Syst. Biol. 14, e8129.
Tompa, P., Davey, N.E., Gibson, T.J., Babu, M.M., 2014. A million peptide motifs for the molecular biologist. Mol. Cell 55, 161–169.
Tonikian, R., Zhang, Y., Sazinsky, S.L., Currell, B., Yeh, J.H., Reva, B., et al., 2008. A specificity map for the PDZ domain family. PLoS Biol. 6, e239.
Uemura, T., Mori, H., Mishina, M., 2004. Direct interaction of GluRdelta2 with Shank scaffold proteins in cerebellar Purkinje cells. Molecular and cellular neurosciences 26, 330–341.
Winn, M.D., Ballard, C.C., Cowtan, K.D., Dodson, E.J., Emsley, P., Evans, P.R., et al., 2011. Overview of the CCP4 suite and current developments. Acta Crystallogr. Sect. D Biol. Crystallogr. 67, 235–242.
Zeng, M., Shang, Y., Guo, T., He, Q., Yung, W.H., Liu, K., et al., 2016. A binding site outside the canonical PDZ domain determines the specific interaction between Shank and SAPAP and their function. Proc. Natl. Acad. Sci. U.S.A. 113, E3081–E3090.
Zhang, Y., Appleton, B.A., Wiesmann, C., Lau, T., Costa, M., Hannoush, R.N., et al., 2009. Inhibition of wnt signaling by dishevelled PDZ peptides. Nat. Chem. Biol. 5, 217–219.
Zhu, Y., Delhommel, F., Cordier, F., Luchow, S., Mechaly, A., Colcombet-Cazenave, B., et al., 2020. Deciphering the unexpected binding capacity of the third PDZ domain of whirlin to various cochlear hair cell partners. J. Mol. Biol. 432, 5920–5937.
Zogzas, C.E., Aschner, M., Mukhopadhyay, S., 2016. Structural elements in the transmembrane and cytoplasmic domains of the metal transporter SLC30A10 are required for its manganese efflux activity. J. Biol. Chem. 291, 15940–15957.